BioNanoScience (2026) 16:181
https://doi.org/10.1007/s12668-026-02430-x

Antibacterial Activity and Acute Cytocompatibility of Green-Synthesized Niobium-Based Nanomaterials Reduced by Ascorbic Acid, Tannic Acid, and Quercetin

Pablo A. Oliveira[1] · Thaís S. Farnesi-de-Assunção[2] · Isabela S. Rotta[2] · Karina F. D. Vicentine[2] · Aline D. Paiva[2] · Dayane S. Alvares[3] · Witor Wolf[4] · Jéferson A. Moreto[4] · Natália B. L. Slade[1]

Received: 27 October 2025 / Accepted: 22 January 2026 / Published online: 16 February 2026

Abstract

Green synthesis represents an environmentally benign and sustainable strategy for producing nanomaterials with enhanced biological functionality and reduced toxicity. Niobium has shown great potential as a biomaterial under physiological conditions. This study aimed to investigate the use of natural antioxidants, ascorbic acid (AA), tannic acid (TA), and quercetin (QUE), as eco-friendly reducing and stabilizing agents in the green synthesis of niobium-based nanomaterials (Nb_{nano}). The obtained nanomaterials were characterized by UV-Vis spectroscopy, Fourier-transform infrared (FTIR) spectroscopy, X-ray diffraction (XRD), scanning-transmission electron microscopy (STEM), scanning electron microscopy coupled with energy-dispersive X-ray spectrometry (SEM-EDX), and zeta potential analysis, indicating the formation of hydrated niobium pentoxide ($Nb_2O_5{\cdot}nH_2O$) nanomaterials with well-preserved structural organization and morphology. Acute cytotoxicity assays using VERO-CCL81 cells revealed that antioxidant-mediated synthesis significantly reduced the toxic effects of Nb_{nano}, increasing their cytocompatibility. All nanomaterials exhibited antibiofilm activity against *Escherichia coli*, effectively reducing bacterial adhesion and biofilm formation. Except for AA-mediated Nb_{nano}, the systems also demonstrated bactericidal activity, revealing their dual action against planktonic and sessile bacterial forms. Overall, the green synthesis of niobium nanomaterials using natural antioxidants represents a sustainable and effective strategy for developing multifunctional materials with promising antibacterial and antibiofilm performance, coupled with reduced cytotoxicity. These findings highlight the potential of niobium-based nanomaterials for biomedical and antifouling applications.

Graphical Abstract

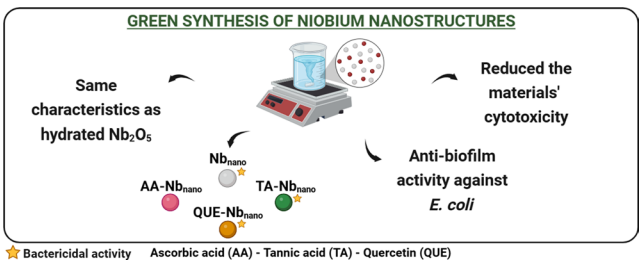

Keywords Green synthesis · Niobium-based nanomaterials · Natural antioxidants · Antibacterial and antibiofilm activity.

Extended author information available on the last page of the article

1 Introduction

The development of nanomaterials with effective antibacterial activity and low toxicity has become a major goal in biomedical and antifouling research. In this context, green synthesis has emerged as a sustainable and versatile approach for producing nanomaterials with enhanced biofunctional properties [1]. Unlike conventional chemical routes, which often require hazardous reagents and generate toxic products, green synthesis employs natural biomolecules as reducing and stabilizing agents, offering a cleaner and safer alternative [1–4]. This eco-friendly strategy not only aligns with environmental principles but also allows the incorporation of biologically active compounds that can improve the antimicrobial performance and biocompatibility of the resulting nanomaterials.

Niobium exhibits notable corrosion resistance and chemical stability, properties that make it particularly attractive for biomedical use under physiological conditions [5]. Nanostructured niobium pentoxide (Nb_2O_5) has been reported to possess low toxicity and potential antimicrobial activity [6–12]. However, studies on its hydrated form, commonly referred to as niobic acid ($Nb_2O_5{\cdot}nH_2O$), have primarily focused on its catalytic performance rather than its biological potential [13, 14]. Among the various synthesis routes for this material, hydrolysis-based methods stand out for their simplicity and rapid processing [15–18]. Alternative approaches include the dissolution of metallic niobium in nitric and hydrofluoric acid mixtures followed by precipitation with ammonium hydroxide [13], the water-in-oil microemulsion technique employing metallic niobium [19], and precipitation from ammonium niobium oxalate using sodium hydroxide [20]. Despite their effectiveness in producing hydrated niobium oxides with diverse morphologies, these conventional methods typically rely on strong acidic or basic reagents, which restrict their applicability in biomedical contexts due to concerns regarding toxicity and environmental impact [13, 19, 20].

Incorporating natural antioxidants such as ascorbic acid (AA), tannic acid (TA), and quercetin (QUE) into the synthesis process provides a promising strategy to overcome the limitations of conventional methods. These biomolecules have been successfully employed as reducing and stabilizing agents in the green synthesis of metal and metal oxide nanoparticles, including selenium with AA [2], silver with TA [3], and titanium dioxide with QUE [4]. Their use has been shown to significantly influence the physicochemical and biological properties of the resulting materials.

For instance, AA-mediated synthesis of selenium nanoparticles produced smaller particles than those obtained using sodium borohydride, while the inclusion of stabilizers such as poly(diallyldimethyl-ammonium chloride) (PDDA) or gelatin further enhanced their antibacterial activity against methicillin-resistant *Staphylococcus aureus* (MRSA) 4591 [2]. However, increased cytotoxicity was also observed, likely associated with the pro-oxidant behavior of AA at higher concentrations. In contrast, TA demonstrated both strong reducing capacity and effective stabilization, yielding colloidal silver nanoparticles that were more stable and concentrated than those synthesized with sodium borohydride [3]. These findings collectively underscore the dual role of natural antioxidants in green synthesis: beyond facilitating nanoparticle formation, they can tailor surface chemistry and biological activity, promoting a synergistic interplay between the intrinsic properties of the metal and the bioactive characteristics of the reducing agent.

In this context, the present study hypothesizes that using AA, TA, and QUE as natural reducing agents in the green synthesis of niobium-based nanomaterials can yield materials with enhanced antibacterial and antibiofilm activity combined with low toxicity. To test this hypothesis, niobium nanomaterials were synthesized in the presence and absence of these antioxidants, characterized in terms of their optical, structural, morphological, and submitted to a preliminary evaluation of their acute cytotoxicity, bactericidal effects, and ability to inhibit *Escherichia coli* biofilm formation. This approach aims to advance the development of sustainable, multifunctional niobium-based systems with potential biomedical and antifouling applications.

2 Materials and Methods

2.1 Synthesis of Niobium-Based Nanomaterials

Nanostructured niobium-based oxides were synthesized via a hydrolysis route by dissolving niobium pentachloride ($NbCl_5$) in deionized water to obtain a final concentration of 25 mg mL^{-1} [17, 18]. This procedure was carried out both in the absence and in the presence of natural antioxidants to compare conventional and green synthesis conditions. For the green synthesis, AA, TA, and QUE were incorporated as reducing and stabilizing agents at a mass ratio of 1:50 (bioactive compound: $NbCl_5$). AA and TA were directly added to the aqueous reaction mixture, whereas QUE was previously dissolved in 1 mL of absolute ethanol before being introduced into the system to ensure complete solubilization [21, 22]. All reactions were continuously stirred at room temperature for 24 h under light-protected conditions. The resulting precipitates were collected by centrifugation at 4000 rpm for 15 min, washed several times with deionized water to remove unreacted residues, and dried in an oven at 80 °C. The dried solids were then finely ground to obtain the nanostructured systems: Nb_{nano} (control, synthesized via hydrolysis), AA-Nb_{nano}, TA-Nb_{nano}, and QUE-Nb_{nano}.

2.2 Structural and Morphological Characterization

X-ray diffraction (XRD) patterns were obtained using a Shimadzu XRD-6100 diffractometer (Kyoto, Japan) equipped with Cu Kα radiation (λ = 1.5406 Å, 40 kV, 30 mA). The measurements were carried out over a 2θ range of 5° to 80° at room temperature after finely grinding the samples to ensure homogeneity. UV-Vis spectra of the materials and the isolated antioxidant compounds were recorded with a Shimadzu UV-1800 spectrophotometer (190–500 nm). The nanomaterials final samples exhibited a concentration of 0.26 mg mL^{-1}, prepared from stock solutions previously dispersed in deionized water (2 mg mL^{-1}) containing 1% Tween 80 and sonicated for 1 h to enhance solubility and dispersion [12, 23, 24]. The spectra of the isolated antioxidants were recorded in distilled water at a concentration of 0.002 mg mL^{-1}, under conditions consistent with those used during synthesis. Fourier transform infrared (FTIR) spectroscopy measurements were performed on a Bruker ALPHA II (Massachusetts, USA) spectrophotometer in the range of 4000–400 cm^{-1}, with 4 cm^{-1} resolution [18]. Both the synthesized materials and the isolated antioxidants were analyzed in the solid state. Scanning Electron Microscopy (SEM) was conducted with a TESCAN VEGA 3 LMU microscope (20 kV) equipped with an energy-dispersive X-ray (EDX) spectrometer to morphologically characterize the produced materials. Imaging was performed in secondary electron (SE) and backscattered electron (BSE) modes [25], after sample metallization with a thin gold coating deposited by sputtering to enhance the materials' electrical conductivity. Scanning-Transmission Electron Microscopy (STEM) was also carried out using a FEI Magellan 400 L SEM equipped with a Field Emission Gun (FEG) source and a STEM detector, operating at 30 kV. The samples were diluted in ethyl alcohol, sonicated and deposited on carbon-coated Cu grids. Micrographs were acquired in Bright-Field (BF), Dark-Field (DF), and Secondary Electron (SE) modes. Zeta potential was determined with a Zetasizer Nano ZS90 (Malvern, UK). The samples were diluted in deionized water (0.5 mg mL^{-1}) containing 1% Tween 80 and subjected to ultrasonic bath treatment. The measurements were carried out in DTS 1060 cuvettes (Malvern) with gold electrodes, employing Doppler velocimetry to determine the zeta potential [12, 26, 27].

2.3 Acute Cytotoxic Effect and Cytotoxic Concentration of the Synthesized Nanomaterials on Mammalian Cell Cultures

The analysis of the in vitro acute cytotoxic effect of niobium-based nanomaterials was performed according to ISO 10993-5:2009 [28]. Briefly, VERO-CCL81 cells were plated in 96-well plates (10^4 cells/well) and the monolayer was exposed for 24 h to different concentrations of the nanoformulations. Cell viability was quantitatively determined through the neutral red uptake (NRU) test and calculated in relation to untreated cells after determining the absorbance at 540 nm, using a microplate reader (Thermo-Plate TpReader, USA) [29]. All experiments were repeated at least three times in independent assays.

Neutral red is a vital water-soluble dye that actively crosses the cell membrane and accumulates in the lysosomes of viable cells via hydrophobic and electrostatic interactions at anionic sites within the lysosomal matrix. Damage to the plasma membrane caused by various substances proportionally reduces the uptake and lysosomal incorporation. Thus, cell viability can be assessed by measuring the intensity of the dye, allowing differentiation between viable, damaged, and/or dead cells [30]. The NRU method, beyond its endorsement by ISO, is also recognized in OECD, is a reliable, low-cost, and reproducible assay with a well-established historical dataset [31, 32].

The mean percentage of cell viability was calculated based on the values relative to untreated cells and plotted against the sample's concentration to generate cell viability curves. The cytotoxic concentration (CC_{50}), defined as the concentration that reduces cell viability by 50%, was determined from these curves. The CC_{50} was determined through non-linear regression using GraphPad prism 8.0 software.

2.4 Antagonistic Activity of the Synthesized Nanomaterials Against *Escherichia coli*

The effect of nanostructured systems on the growth of *Escherichia coli* ATCC 25922 was evaluated using the broth microdilution method. Niobium-based nanomaterials (2,500 to 156.25 μg mL^{-1}; 50 μL) or pure antioxidants (corresponding to a 1:50 mass ratio of bioactive compound to $NbCl_5$, i.e., 50 to 3.125 μg mL^{-1}) were added to polystyrene microplates containing BHI broth (2x concentration; 50 μL), followed by stationary-phase *E. coli* inoculum (10^6 CFU mL^{-1}; 10 μL). Plates were incubated at 37 °C for 24 h under aerobic conditions. Negative control wells containing uninoculated BHI broth, and positive controls containing only *E. coli* and BHI broth were included. The minimum inhibitory concentration (MIC) was defined as the lowest concentration inhibiting bacterial growth [33]. The minimal bactericidal concentration (MBC) was determined by subculturing aliquots (5 μL) from wells showing no bacterial growth onto BHI agar plates, which were incubated at 37 °C for 24 h under aerobic conditions. The MBC was defined as the lowest concentration that prevented bacterial growth [34].

Biofilm-forming capacity of *E. coli* ATCC 25922 was assessed in the absence and presence of the synthesized

materials using the crystal violet assay in polystyrene microplates. Stationary-phase bacterial suspensions (0.5 McFarland; 10 µL) were added to the wells already containing BHI broth (2x; 50 µL), and co-cultured with the nanostructured materials or pure antioxidants (2x MIC, MIC, 0.5x MIC; 50 µL). The samples were incubated at 37 °C for 24 h under aerobic conditions. Subsequently, the microplates were treated with methanol (75%; 15 min) and stained with crystal violet solution (0.25%; 150 µL). The plates were kept at room temperature for 30 min, and the adhered dye was subsequently extracted with ethanol (95%; 150 µL). Absorbance was measured at 540 nm using a microplate reader [35].

To avoid potential interference caused by the physical presence or adhesion of the nanomaterials to the polystyrene plates and ensure that colorimetric readings were not affected by this factor, control wells containing only the nanomaterials and BHI medium, without *E. coli* suspension, were included.

2.5 Statistical Analysis

All statistical evaluations were carried out using Microsoft Excel for Windows and GraphPad Prism software (version 8.0; GraphPad Software, La Jolla, CA, USA). Data distribution was assessed and confirmed to follow a Gaussian pattern. Consequently, one-way ANOVA with Dunn's post hoc test was applied for comparisons on cell viability. ANOVA followed by Tukey's multiple comparisons test to determine the influence of the niobium-based nanomaterials on biofilm formation capacity. Results were expressed as mean ± standard deviation, with statistical significance set at $p < 0.05$.

3 Results and Discussion

X-ray diffraction (XRD) analyses were conducted to examine the structural organization of the synthesized niobium-based nanomaterials. The results are presented in Fig. 1a and show that the niobium-based materials synthesized both via hydrolysis and mediated by natural antioxidants exhibit similar XRD patterns, which are characterized by two broad diffraction peaks around 26° and 54°. These profiles are consistent with those reported in the literature for hydrated niobium pentoxide ($Nb_2O_5 \cdot nH_2O$) [12, 15, 17, 36], in which the absence of sharp reflections is indicative of amorphous or very low-crystallinity structures [17, 18, 36–38]. The patterns observed here are therefore consistent with amorphous $Nb_2O_5 \cdot nH_2O$ generated under mild solution-based synthesis conditions. Although AA-Nb_{nano} and TA-Nb_{nano} show a slight peak near 10°, the presence of antioxidants does not significantly alter the fundamental structural characteristics of the materials. It is worth emphasizing that, due to the amorphous nature of the synthesized materials, it was not possible to correlate the obtained XRD profiles with any established reference pattern, in line with Souza et al. findings [39]. Altogether, the XRD data suggests that all samples correspond to amorphous niobium pentoxide, in agreement with previous findings reported by our research group for similar hydrolysis-derived niobium nanomaterials [12].

UV-Vis spectroscopy was employed to evaluate the optical properties of the synthesized materials. The resulting spectra, together with those of the isolated antioxidants, are presented in Fig. 1b-d. The Nb_{nano} spectra display a shoulder near 265 nm and a peak around 310 nm, features that are characteristic of Nb_2O_5 and $Nb_2O_5 \cdot nH_2O$ [12, 37, 40]. These oxides, identified as Nb_2O_5-based nanomaterials, are intrinsically wide-bandgap dielectric/semiconductor materials rather than plasmonic noble metals (e.g., gold or silver). Owing to their electronic structure, the valence electrons in these nanomaterials are strongly localized and bound to the atomic lattice, instead of forming a free-electron gas [41, 42]. Consequently, these nanoparticles do not exhibit a characteristic localized surface plasmon resonance (LSPR) in the visible region of the electromagnetic spectrum. Figure S1 presents the UV-Vis absorption spectra of niobium oxide based-nanomaterials dispersions at different concentrations, ranging from 0.05 to 0.75 mg mL^{-1}. Variations in concentration do not lead to the emergence of any LSPR-related absorption feature, confirming that such a response is intrinsically absent in this material system. The spectral profiles remain essentially unchanged across all dilutions, supporting the conclusion that the observed optical response is governed by semiconductor behavior. Accordingly, the analysis is focused on determining the optical band gap rather than on plasmonic phenomena. This spectral pattern was also observed for all the nanostructured materials obtained in the presence of antioxidants as reducing agents. Nevertheless, a blue shift is observed in relation to the 310 nm peak, with AA-Nb_{nano} (Fig. 1b) and TA-Nb_{nano} (Fig. 1c) shifting to 300 nm and 302 nm, respectively. These spectral variations can be attributed to changes in the morphological characteristics of the nanomaterials, such as differences in the size and shape of the nanoparticles [43]. The characteristic bands of the reducing agents are not observed in the synthesized material. This behavior can be attributed both to the overlapping absorbance of niobium pentoxide with that of the respective antioxidants and to the possible removal of the latter during the washing step of the synthesis process. In conjunction with the XRD data, these results indicate that the use of natural antioxidants enables the successful synthesis of niobium-based materials while preserving the intrinsic optical properties of Nb_2O_5.

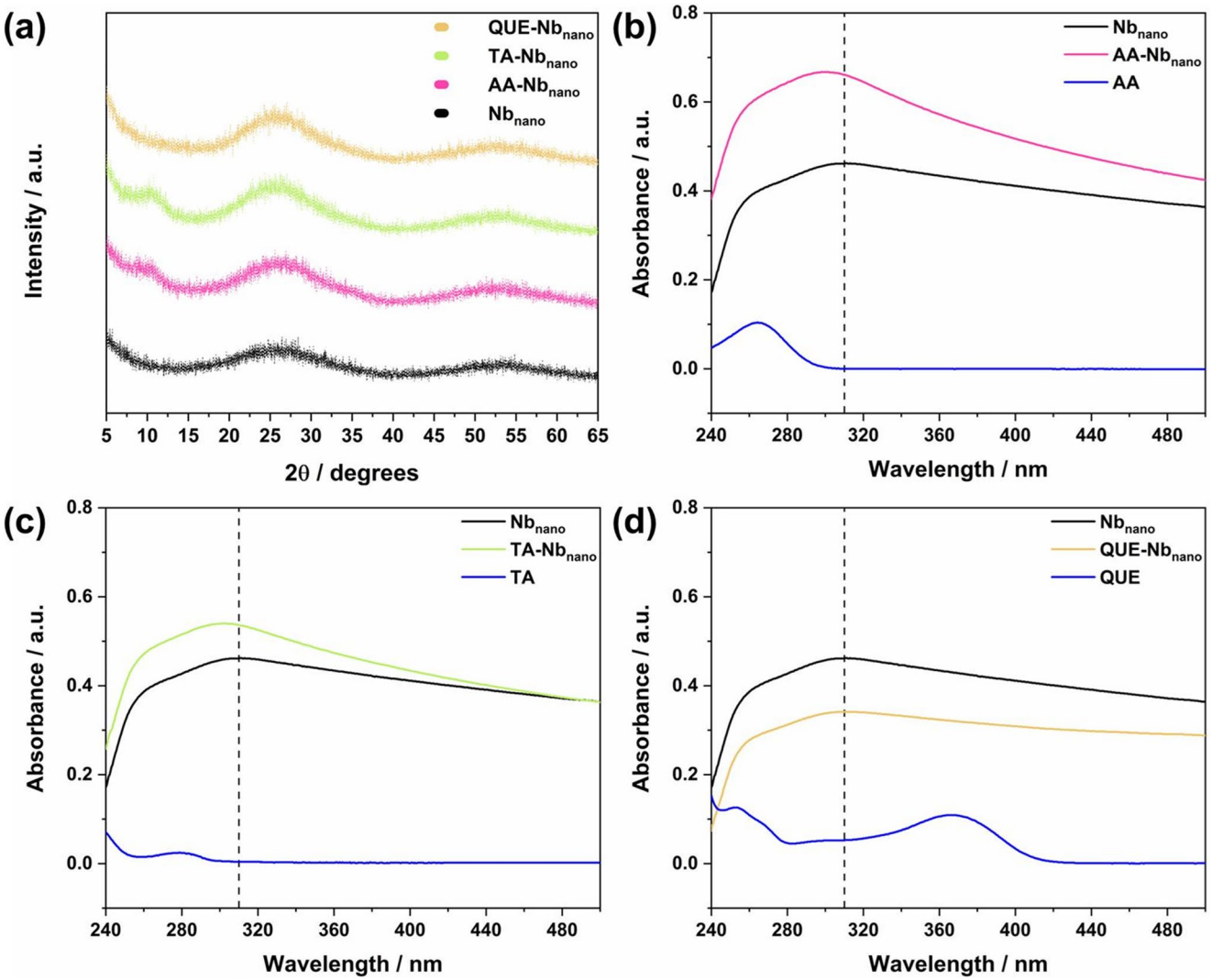

Fig. 1 (**a**) X-ray diffraction (XRD) patterns and (b-d) UV-Vis spectra of the Nb_{nano} and the green-synthesized (**b**) AA-Nb_{nano}, (**c**) TA-Nb_{nano}, and (**d**) QUE-Nb_{nano}, in addition to the spectra recorded for the isolated antioxidants

Fourier-transform infrared (FTIR) spectroscopy was employed to investigate the structural characteristics of the synthesized materials. The resulting spectra are presented in Fig. 2, which displays AA-Nb_{nano} (Fig. 2a), TA-Nb_{nano} (Fig. 2b), and QUE-Nb_{nano} (Fig. 2c), along with the spectra of Nb_{nano} (synthesized via hydrolysis) and the respective isolated antioxidants. Nb_{nano} exhibits characteristic bands at 3040 and 1606 cm^{-1}, corresponding to the O–H stretching and bending vibrations of water molecules incorporated into the material [38, 44, 45]. Additional bands at 856 and 540 cm^{-1} are attributed to Nb = O bonds and Nb–O vibrations, respectively [18, 36, 38, 46]. Bands observed at 1236 and 1158 cm^{-1} indicate the presence of residual organic components from the synthesis process [38, 47]. These results are consistent with previous studies on $Nb_2O_5{\cdot}nH_2O$ [12, 18, 44, 48]. The FTIR spectra of AA-Nb_{nano}, TA-Nb_{nano}, and QUE-Nb_{nano} display patterns similar to those of Nb_{nano}, confirming the presence of functional groups characteristic of niobium oxide. Consistent with the XRD and UV-Vis results, these observations indicate that, despite variations in the synthesis method, all materials retain the features of hydrated niobium oxide. Furthermore, FTIR analysis revealed additional bands corresponding to organic groups associated with the green synthesis process. As shown in Fig. 2, AA-Nb_{nano} exhibits C–O bond vibrations and C–H bending vibrations, while TA-Nb_{nano} and QUE-Nb_{nano} display C = C stretching vibrations associated with aromatic groups [47, 49]. These characteristic bands, observed in the ranges of 1600–1400 cm^{-1} and 1300 − 1000 cm^{-1}, indicate the presence of chemical groups related to the structures of the antioxidant compounds. Additionally, QUE-Nb_{nano} presents a band at 2980 cm^{-1}, which can be attributed to the C–H stretching vibration of QUE. These variations in the FTIR spectra of the synthesized materials are similar to

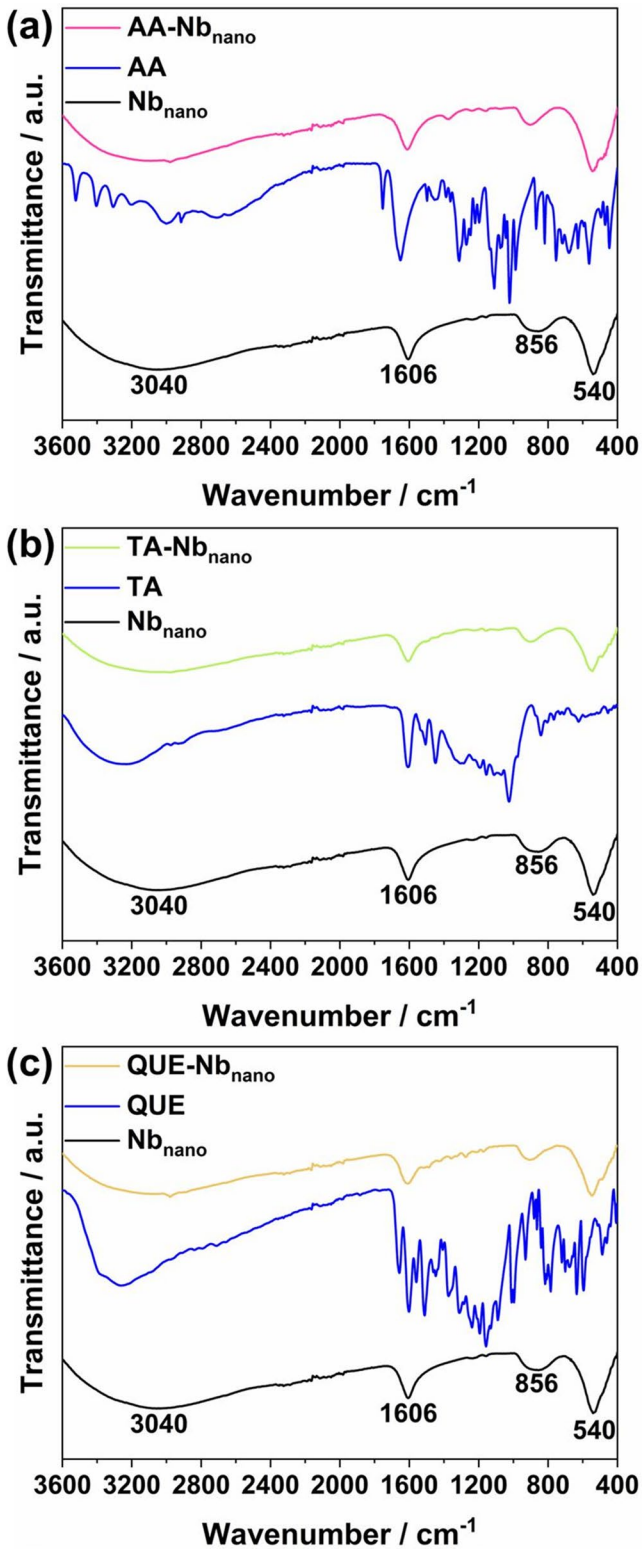

Fig. 2 FTIR spectra of the Nb_{nano} and the green-synthesized samples: (**a**) AA-Nb_{nano}, (**b**) TA-Nb_{nano}, and (**c**) QUE-Nb_{nano}, along with the spectra of the antioxidants in their isolated forms

those reported by Chahardoli and colleagues [4] for titanium dioxide nanoparticles synthesized using QUE as a reducing agent, where they observed the emergence of bands associated with C = C and C-H bonds of the antioxidant compound. In this context, these results indicate that materials obtained via green synthesis retain the fundamental characteristics of the hydrolysis-derived material, while also incorporating prominent organic groups originating from the reducing agents.

SEM analyses were used to investigate the morphology of the synthesized materials, Fig. 3. The material obtained via hydrolysis is shown in Fig. 3a, along with its chemical composition determined by energy-dispersive X-ray spectroscopy (EDX) (Fig. 3b). The micrograph reveals the presence of Nb_{nano} clusters with poorly defined shapes, consistent with reports for $Nb_2O_5{\cdot}nH_2O$ samples [12, 36]. The difficulty in distinguishing the morphology of the nanomaterials may also be attributed to the inherently low electrical conductivity of niobium pentoxide [50]. Even after gold (Au) nanoparticle deposition, image acquisition remained challenging, as these materials are prone to structural damage during attempts to improve image resolution. The EDX analysis confirms that the material is mainly composed of niobium (Nb) and oxygen (O), with trace amounts of chlorine (Cl) remaining from the $NbCl_5$ precursor (Fig. 3b). The material produced via green synthesis is represented in Fig. 3c and d by the micrograph and EDX spectrum of the QUE-Nb_{nano} sample, respectively. The incorporation of QUE during synthesis did not significantly modify the morphological characteristics of the material compared to that obtained via hydrolysis. However, compositional analysis revealed that, in addition to the main elements Nb and oxygen O, a substantial amount of carbon (C) was also present. This result corroborates the FTIR spectroscopy findings, as it demonstrates that the green synthesis was effective in obtaining a niobium-based nanomaterial enriched with elements characteristic of reducing agents, which may contribute to its stability and effectiveness in aqueous media.

To further investigate the morphological properties of the synthesized materials, STEM analyses are presented in Fig. 4. The results reinforce the presence of clusters composed of nanometric particles, regardless of the antioxidant compound used in the synthesis. This observation is consistent with previously reported hydrated niobium oxides synthesized using similar methodologies [12, 15, 17, 18]. The obtained micrographs were processed and analyzed using ImageJ software (version 1.54 g) to determine the distribution pattern of the synthesized nanomaterials (Figure S2). The particle diameter was estimated based on the Feret's

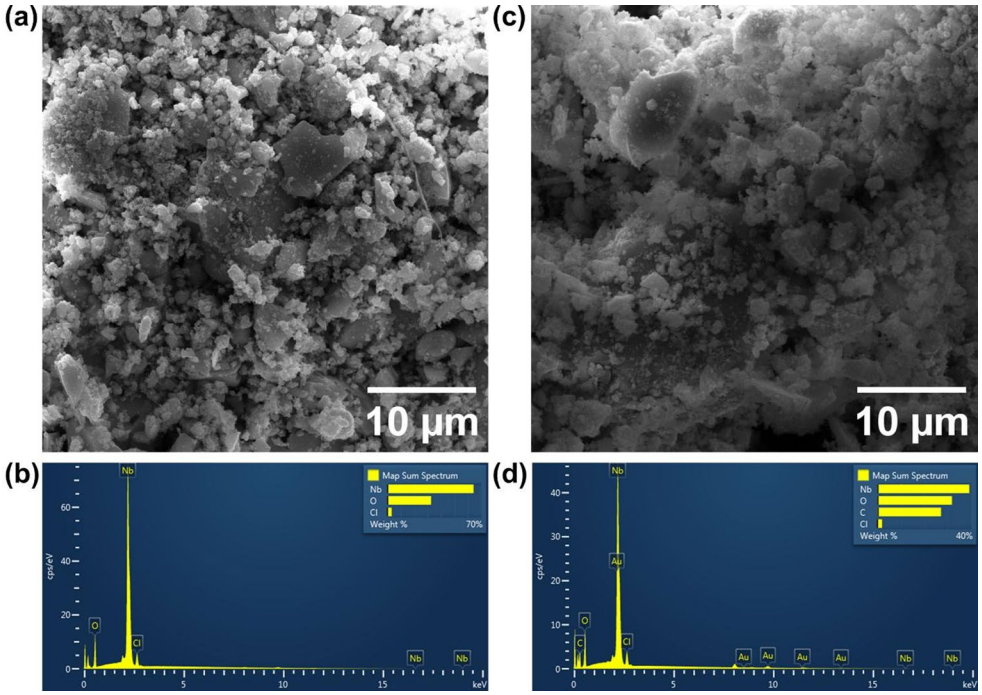

Fig. 3 (**a**) Representative SEM image, and (**b**) EDX spectrum of Nb_{nano}. (**c**) Representative SEM image, and (**d**) EDX spectrum of sample synthesized with QUE ($QUE\text{-}Nb_{nano}$). Magnification: 5,000x. The Au signal originates exclusively from the sputter-coating process; differences in visualization settings between panels account for its appearance in some spectra

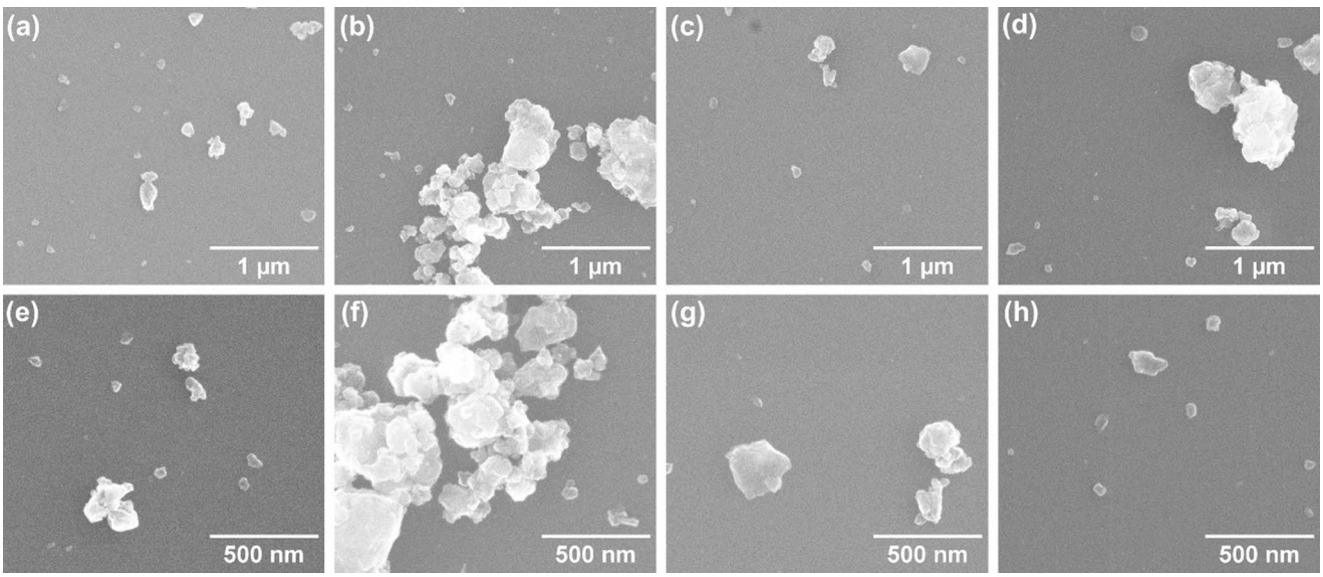

Fig. 4 Representative STEM images acquired in SE mode of (**a**) Nb_{nano} and the green-synthesized samples: (**b**) $AA\text{-}Nb_{nano}$, (**c**) $TA\text{-}Nb_{nano}$, and (**d**) $QUE\text{-}Nb_{nano}$, magnification of 100,000x. Representative STEM images acquired in SE mode of (**e**) Nb_{nano}, (**f**) $AA\text{-}Nb_{nano}$, (**g**) $TA\text{-}Nb_{nano}$, and (**h**) $QUE\text{-}Nb_{nano}$, 200,000x magnification

diameter, defined as the distance between two parallel tangents to the particle contour in a specific direction [51]. This parameter is particularly suitable for the characterization of particles with irregular morphologies or low sphericity [52, 53]. The Nb_{nano} material exhibited particles with an average size of approximately 24 ± 3 nm, whereas $QUE\text{-}Nb_{nano}$ showed an average diameter of around 13 ± 9 nm, revealing the presence of distinct particle populations with sizes on the order of 7 ± 1 nm, 14 ± 1 nm, and 26 ± 2 nm. Due to the pronounced presence of aggregates in the $AA\text{-}Nb_{nano}$ and $TA\text{-}Nb_{nano}$ systems, it was not possible to obtain satisfactory statistics for determining their average size. Nevertheless, particles with dimensions of approximately 45 nm for $AA\text{-}Nb_{nano}$ and 50 nm for $TA\text{-}Nb_{nano}$ could be identified. Although it was not possible to determine the specific size and morphology of the synthesized materials, the morphological analyses obtained via STEM indicate that all materials are in the nanometric scale.

Zeta potential measurements were performed to evaluate the properties of surface charge and stability of the synthesized materials in aqueous dispersions. The Nb_{nano} sample exhibited anionic behavior, with an average zeta potential of −18.1 ± 0.9 mV. This value is notably more negative than those typically reported for Nb_2O_5, which range from below − 10 mV to approximately − 5 mV [54, 55]. Such discrepancies are likely attributable to variations in synthesis methods and differences in the structural organization of the samples. The use of the natural antioxidants in the synthesis induced slight variations in the zeta potential. The average zeta potential values obtained for TA-Nb_{nano} and QUE-Nb_{nano} were − 14.1 ± 1.1 mV and − 13.4 ± 0.5 mV, respectively, whereas AA-Nb_{nano} exhibited a slightly more negative value of −18.8 ± 0.9 mV. Despite the differences in the electrical charge and hydrophobicity of the reducing agents [56], these variations did not modify the overall anionic electrostatic nature of the material. However, it is possible to note that the most hydrophilic reducing agent, AA, induced minimal changes in the zeta potential compared to the Nb_{nano}, while the most hydrophobic compound, QUE, led to the greatest deviation. This suggests that the hydrophobicity of the reducing agent may influence its interaction with the particle surface, thereby affecting surface charge distribution.

It is worth noting that, in a previous study, the post-synthesis functionalization of Nb_{nano} with natural antioxidants resulted in significantly more negative zeta potentials (−24.8 mV for Nb-AA, −24.1 mV for Nb-TA, and − 27.8 mV for Nb-QUE) [12]. These values reflect the adsorption of anionic bioactive compounds onto the nanostructure surface at neutral pH and are consistent with the formation of metal-antioxidant complexes mediated by hydroxyl groups on hydrated niobium oxides [12]. In this context, surface functionalization increased the density of negative surface charges due to the presence of ionizable functional moieties from the adsorbed molecules [12]. In contrast, when the same antioxidants were employed as reducing agents during green synthesis, only moderate changes in zeta potential were observed. The less negative values compared to the functionalized samples suggest a distinct interaction mechanism, in which the antioxidants participate in the nucleation and growth of the nanomaterials rather than merely adsorbing onto their surface. During this synthesis process, the antioxidants likely act as both reducing and stabilizing agents, promoting the partial incorporation of functional groups, such as hydroxyl or carbonyl moieties, into the oxide matrix. This incorporation can modify the surface chemistry and influence particle stabilization through electrostatic and steric effects, even in the absence of extensive surface coupling of the bioactive molecules. Overall, these findings highlight the distinct roles of natural antioxidants in post-synthesis functionalization versus green synthesis approaches, while reaffirming the effectiveness of the latter in producing niobium-based nanomaterials through a simple, low-cost, and environmentally sustainable route with strong potential for scalable production.

Niobium-based nanomaterials were evaluated regarding acute cytotoxicity potential in vitro, using VERO-CCL81 cell line (Fig. 5). The acute cytotoxicity assays must be performed within 24 h, in accordance with established regulatory guidelines (ISO 10993-5:2009) [28]. This time helps preserve the viability of the culture and avoid damage that can occur due to nutrient depletion and the accumulation of residual metabolites at longer exposure times. Furthermore, acute toxicity assays provide early insight into mechanisms of cellular damage and enable rapid screening for estimating initial doses for in vivo toxicity studies [57]. The results indicate that the blank sample, Nb_{nano}, exhibited a significant cytotoxic effect at concentrations above 62.5 μg mL^{-1}, with an average reduction in cell viability of approximately 17% at his dose compared to untreated controls (Fig. 5a). In contrast, samples synthesized with natural antioxidants, AA-Nb_{nano}, TA-Nb_{nano}, and QUE-Nb_{nano}, did not induce a statistically significant reduction in VERO cell viability at the same concentration (62.5 μg mL^{-1}), as compared to untreated cells ($p > 0.05$) (Fig. 5b and c, and 5d, respectively).

The cytotoxicity concentration (CC_{50}) represents the concentration of a compound required to reduce cell viability by 50%. It was determined from a dose-response curve generated using the cell viability data. In addition, the use of CC_{50} allows the comparison of different substances according to their biological potency, making it possible to classify different nanomaterials as more or less biocompatible. After 24 h exposure, the CC_{50} was 91.31 μg mL^{-1} for Nb_{nano} (Fig. 6a), 94.31 μg mL^{-1} for AA-Nb_{nano} (Fig. 6d), 112.6 μg mL^{-1} for QUE-Nb_{nano} (Fig. 6c), and 120.6 μg mL^{-1} for TA-Nb_{nano} (Fig. 6b). These data indicate that the use of AA, TA, and QUE as reducing agents mitigates the cytotoxicity of niobium-based nanomaterials, as compared to the material synthesized without them, as evidenced by the higher CC_{50} values observed for the nanomaterials obtained via green synthesis.

Contact of xenobiotic materials with living organisms can lead to deleterious damage that affects the structure of the plasma and lysosomal membrane and thus cause irreversible damage to cell biology [58]. In contrast, natural antioxidants are consumed through food and are widely known for their ability to minimize the effects resulting from the production and accumulation of free radicals generated after cellular stress [59]. Our findings are in line with the literature reports indicating that nanomaterials synthesized with antioxidants exhibit improved biocompatibility and enhanced biological safety [60–62].

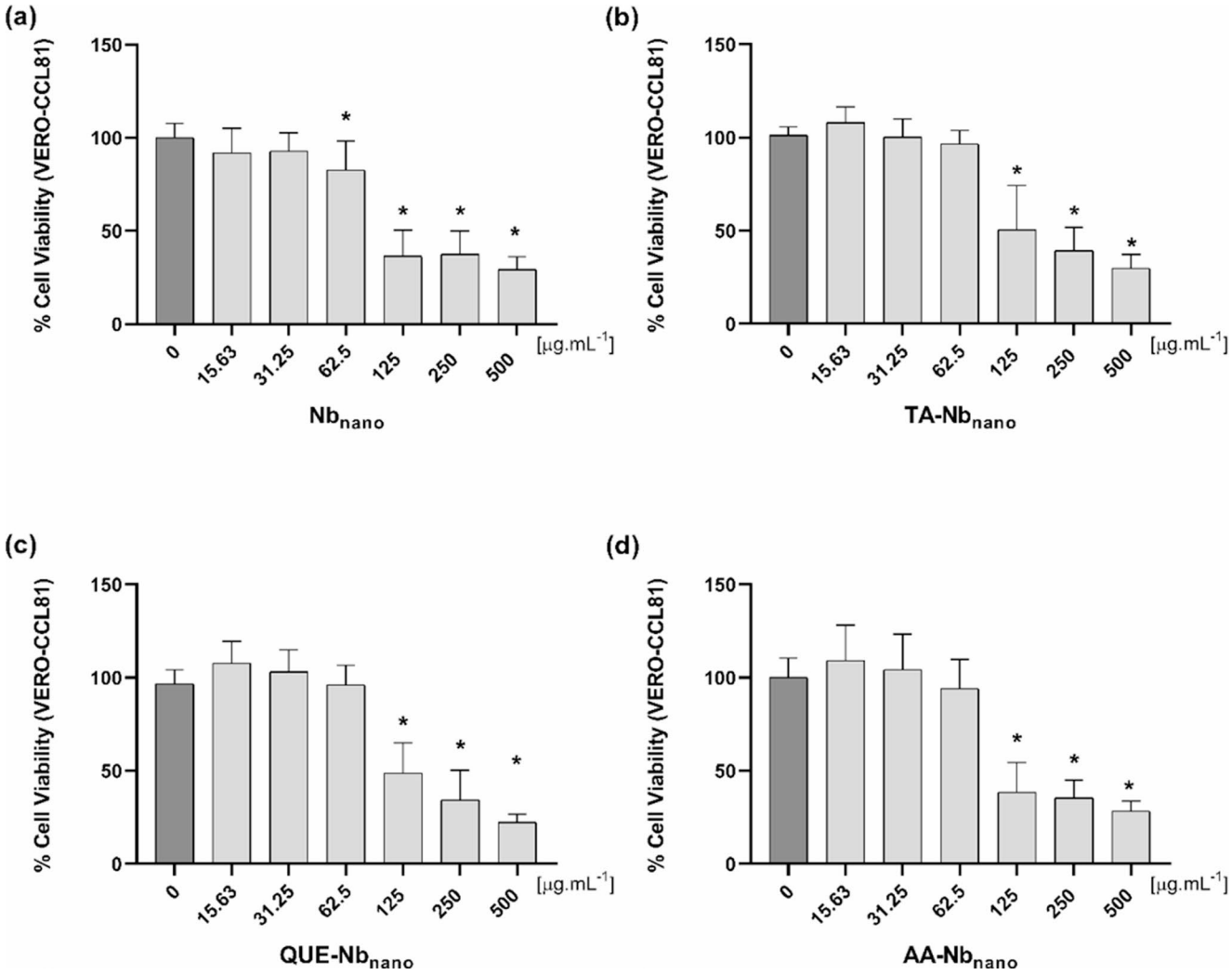

Fig. 5 Cell viability comparison of niobium-based nanomaterials at different concentrations (15.63 to 500 µg mL^{-1}) in VERO-CCL81 cell line, at 24 h. (**a**) Nb_{nano}, (**b**) TA-Nb_{nano}, (**c**) QUE-Nb_{nano} and (**d**) AA-Nb_{nano}. *indicates significant differences, compared to the untreated group. Statistical differences were assessed using one-way ANOVA followed by Dunn's post hoc test ($p < 0.05$). All concentrations were tested in triplicate across at least three independent experiments

Despite the scarcity of in vivo studies addressing local and systemic effects resulting from the use of niobium, Dsouki et al. [63] demonstrated no significant hematological and hepatic changes. Kiyochi Jr. et al. [64] demonstrated that materials based on niobium pentoxide have desirable characteristics for a good biomaterial. Furthermore, joint inoculation of NbO_3 nanoparticles does not result in systemic dissemination to vital organs and promotes the production of anti-inflammatory cytokines, suggesting potential immunomodulatory activity.

The niobium-based nanomaterials showed antagonistic activity against *E. coli* ATCC 25922. The bioactive compounds and nanostructured systems were able to inhibit the growth of *E. coli*, and a concentration of 625 µg mL^{-1} was defined as MIC for all isolated compounds, as well as for Nb_{nano}, TA-Nb_{nano} and QUE-Nb_{nano}. Only AA-Nb_{nano} showed a MIC value of 1,250 µg mL^{-1} (Table 1). The MBC value against *E. coli* was defined as 2,500 µg mL^{-1} (four times higher than the MIC), except for AA and Nb-AA, for which the MBC could not be determined, since bacterial colonies were observed even at 2,500 µg mL^{-1} (maximum concentration evaluated). These results suggest that TA-Nb_{nano} and QUE-Nb_{nano} have a bactericidal effect, while AA-Nb_{nano} is bacteriostatic against *E. coli*.

The differences observed between the MIC/MBC and CC_{50} values can be explained by the intrinsic biological differences between bacterial and mammalian cells. *E. coli*, as a Gram-negative bacterium, possesses a complex cell envelope that includes an outer membrane acting as an effective permeability barrier, thereby requiring higher concentrations of the nanomaterials to achieve inhibitory (MIC) or bactericidal (MBC) effects. In contrast, the mammalian

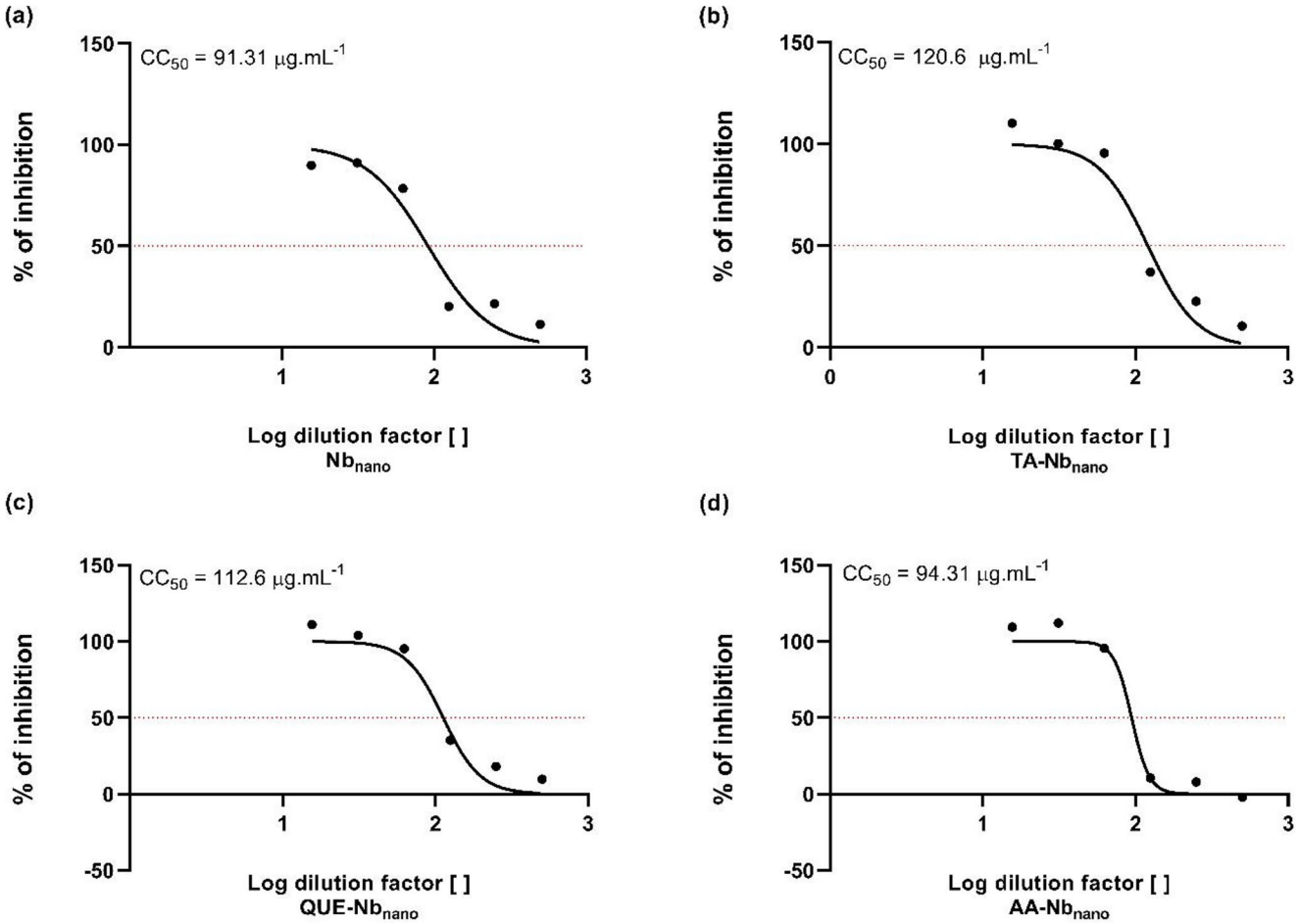

Fig. 6 Cytotoxic concentration 50% (CC_{50}) of niobium-based nanomaterials in Vero-CCL81 cells after 24 h of exposure. The graphs display the dose-response curves used to calculate CC_{50} values, with concentrations presented on a logarithmic scale. (**a**) Nb_{nano}, (**b**) TA-Nb_{nano}, (**c**) QUE-Nb_{nano} and (**d**) AA-Nb_{nano}

Table 1 Minimum inhibitory concentration (MIC) and minimum bactericidal concentration (MBC) of niobium-based nanomaterials against *Escherichia coli* ATCC 25922

Compounds	MIC (µg mL^{-1})	MBC (µg mL^{-1})
Nb_{nano}	625	2,500
TA	625	2,500
TA-Nb_{nano}	625	2,500
QUE	625	2,500
QUE-Nb_{nano}	625	2,500
AA	625	-
AA-Nb_{nano}	1,250	-

cells used in the cytotoxicity assays contain only a single plasma membrane and lack comparable protective structures, making them inherently more susceptible to external agents. Thus, the lower CC_{50} values reflect expected differences in membrane architecture, permeability, and cellular resilience, rather than indicating disproportionate toxicity of the nanomaterials.

A significant decrease in the *E. coli* biofilm-forming capacity was observed in the presence of the niobium-based nanomaterials at all tested concentrations (2,500 to 312 µg mL^{-1}), compared with the non-exposed control biofilms ($p<0.05$) (Fig. 7). It is important to highlight that TA-Nb_{nano}, demonstrated superior anti-biofilm activity at the concentrations corresponding to MIC and 0.5x MIC (625 and 312 µg mL^{-1}, respectively), showing significantly greater efficacy than the pure compound TA at the same concentrations ($p<0.05$) (Fig. 7b). Specifically, at the MIC (625 µg mL^{-1}), TA-Nb_{nano} inhibited biofilm formation by 97.3% compared to 77.4% for TA. Similarly, at 0.5x MIC (312 µg mL^{-1}), inhibition rates were 94.7% for TA-Nb_{nano} and 66.6% for TA. This result is particularly relevant, as it demonstrates that the incorporation of TA not only enhances the anti-biofilm activity of the nanomaterial but also contributes to its biocompatibility as evidenced to highest CC_{50} value (Fig. 6b). In contrast, the anti-biofilm activity of QUE-Nb_{nano} or AA-Nb_{nano} did not significantly differ from

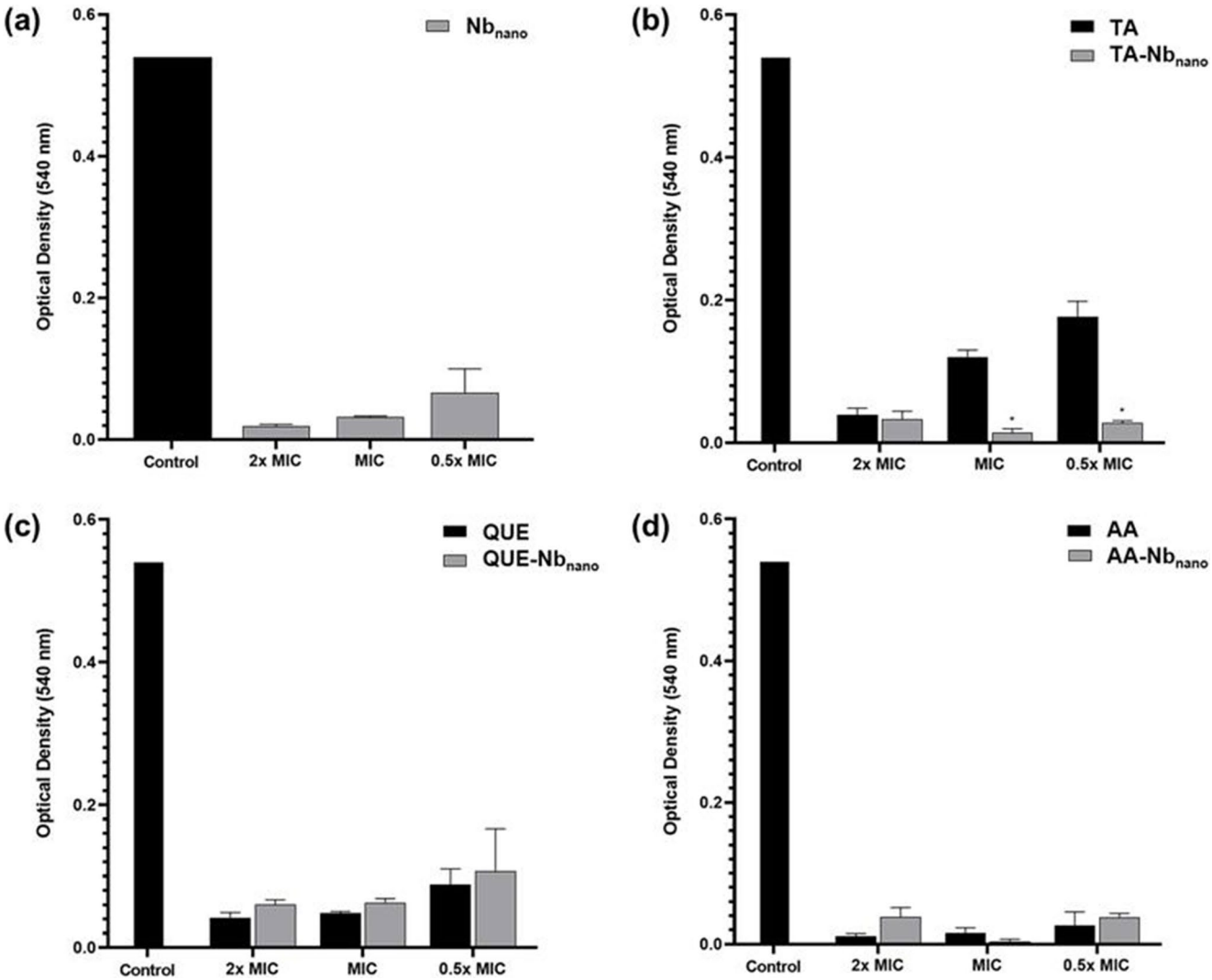

Fig. 7 Effect on the reduction of *Escherichia coli* ATCC 25922 biofilm formation by niobium-based nanomaterials at different concentrations (2x MIC, MIC and 0.5x MIC). (**A**) Nb_{nano}, (**B**) TA and its combination with Niobium (TA-Nb_{nano}), (**C**) QUE and QUE-Nb_{nano}, (**D**) AA and AA-Nb_{nano}. *indicates significant differences, compared to the isolated compound at the same concentration, according to Tukey's multiple comparisons test ($p < 0.05$)

those of their isolated counterparts ($p > 0.05$) (Fig. 7c and d, respectively).

The ability of bacteria to form biofilms significantly contributes to their persistence and resistance to antimicrobial compounds and to the immune system [65, 66]. This adaptive feature poses a challenge in controlling microbial contamination, both in industrial and clinical environments. Different metal-based compounds have demonstrated antagonistic and anti-biofilm activity against *E. coli* [67–70]. In our study, the niobium-based nanomaterials exhibited significant antibacterial activity against *E. coli* ATCC 25922, and effectively inhibited biofilm formation, with inhibition levels ranging from 66.6% to 99.1%, depending on the concentration evaluated. These findings align with previous studies highlighting the efficacy of nanoparticles in combating biofilm-associated infections [71–73]. For instance, it has been suggested that following bacterial attachment to surfaces, the released quercetin disrupts the bacterial membrane, enabling silver nanoparticles (AgNPs) to penetrate the cell wall and membrane, effectively killing the bacteria and preventing biofilm formation [71]. Al-Sawarees and colleagues [72] also demonstrated the capacity of silver nanoparticles, triclosan, and trans-cinnamaldehyde in effectively inhibiting biofilm formation by *S. aureus* and *E. coli*. Similarly, it was observed that ellagic acid-bonded magnetic nanoparticles reduced *E. coli* biofilm formation by 43–62% when compared to the control [73].

Despite the encouraging outcomes obtained, it remains imperative to further investigate the interactions between niobium-based nanomaterials synthesized through green

methodologies and bacterial biofilm systems, with the objective of elucidating the molecular and physicochemical mechanisms underlying their biological activity. The present work provides a conceptual framework demonstrating that natural antioxidant compounds, differing in molecular dimensions and chemical characteristics, can function as effective reducing and stabilizing agents in the environmentally benign synthesis of niobium nanomaterials. Beyond validating the feasibility of this green approach, the findings emphasize the broader technological and biomedical relevance of these materials, as their sustainable production aligns with the principles of eco-efficient nanotechnology and offers promising perspectives for the development of advanced antibiofilm and biocompatible systems.

4 Conclusions

In conclusion, the present work establishes a sustainable synthetic route for producing niobium-based nanomaterials by employing antioxidant molecules as reducing and functionalizing agents. This approach proved effective in preserving the morphological and structural integrity of hydrated niobium pentoxide, while simultaneously enhancing its biological performance. The inclusion of natural antioxidants markedly reduced acute cytotoxicity and promoted inhibitory activity against *Escherichia coli* biofilm formation, demonstrating that green synthesis can provide safer and functionally improved nanomaterials. These outcomes not only reinforce the potential of niobium oxides in biomedical and environmental applications but also emphasize the relevance of integrating bioactive compounds into nanomaterial design. Future investigations should focus on elucidating the mechanistic interactions between antioxidant species and niobium surfaces, as well as assessing their performance in complex biological systems. Such efforts will be essential to advance the practical translation of these green-synthesized nanomaterials toward therapeutic and technological innovations.

Supplementary Information The online version contains supplementary material available at https://doi.org/10.1007/s12668-026-02430-x.

Acknowledgements This work was supported by the Foundation Coordination for the Improvement of Higher Education Personnel (CAPES - Finance Code 001); the National Council for Scientific and Technological Development (CNPq-Brazil) (Grants 402988/2021-3, 302770/2022-4, and 405457/2023-5); the São Paulo Research Foundation (FAPESP) (Grants 2024/02504-0 and 2022/07231-7); the Minas Gerais StateAgency for Research and Development (FAPEMIG-Brazil) (Processes APQ-00554-21, APQ-00458-24, and RED-00116-23); and the University of São Paulo for the financial support through the announcement for new faculty members.

Author Contributions Pablo A. Oliveira: Investigation, Formal analysis, and Writing – original draft. Thaís S. Farnesi-de-Assunção: Investigation, Formal analysis. Isabela S. Rotta: Investigation, Formal analysis. Karina F. D. Vicentine: Investigation, Formal analysis. Aline D. Paiva: Investigation, Formal analysis. Dayane S. Alvares: Investigation, Formal analysis. Witor Wolf: Investigation, Formal analysis. Jéferson (A) Moreto: Writing – review and editing, Funding acquisition, Formal analysis. Natália (B) L. Slade: Funding acquisition, Project administration, Writing – review and editing. All authors have given approval to the final version of the manuscript.

Funding The Article Processing Charge (APC) for the publication of this research was funded by the Coordenação de Aperfeiçoamento de Pessoal de Nível Superior - Brasil (CAPES) (ROR identifier: 00x0ma614). This work was supported by the Foundation Coordination for the Improvement of Higher Education Personnel (CAPES - Finance Code 001); the National Council for Scientific and Technological Development (CNPq-Brazil) (Grants 402988/2021-3, 302770/2022-4, and 405457/2023-5); the São Paulo Research Foundation (FAPESP) (Grants 2024/02504-0 and 2022/07231-7); the Minas Gerais State Agency for Research and Development (FAPEMIG-Brazil) (Processes APQ-00554-21, APQ-00458-24, and RED-00116-23); and the University of São Paulo for the financial support through the announcement for new faculty members.

Data Availability All data generated or analyzed during this study are included in this published article and its supplementary information files.

Code availability Not applicable.

Declarations

Ethical Approval Not applicable.

Research Involving Humans and Animals Statement Not applicable.

Informed Consent Not applicable.

Competing Interests The authors declare no competing interests.

References

1. Singh, J., Dutta, T., Kim, K. H., Rawat, M., Samddar, P., & Kumar, P. (2018). 'Green' synthesis of metals and their oxide nanoparticles: Applications for environmental remediation. *Journal Of Nanobiotechnology, 16*, Article 84. https://doi.org/10.1186/s12951-018-0408-4

2. Bužková, A., Hochvaldová, L., Večeřová, R., Malina, T., Petr, M., Kašlík, J., Kvítek, L., Kolář, M., Panáček, A., & Prucek, R. (2025). Selenium nanoparticles: Influence of reducing agents on particle stability and antibacterial activity at biogenic concentrations. *Nanoscale*, *17*, 8170–8182. https://doi.org/10.1039/D4NR05271D
3. Cataldo, F., Ursini, O., & Angelini, G. (2013). A green synthesis of colloidal silver nanoparticles and their reaction with ozone. *European Chemical Bulletin, 2*(10), 700–705.
4. Chahardoli, A., Jalilian, F., Shokoohinia, Y., & Fattahi, A. (2023). The role of quercetin in the formation of titanium dioxide nanoparticles for nanomedical applications. *Toxicology In Vitro, 87*, Article 105538. https://doi.org/10.1016/j.tiv.2022.105538
5. Safavi, M. S., Walsh, F. C., Visai, L., & Khalil-Allafi, J. (2022). Progress in Niobium Oxide-Containing Coatings for Biomedical Applications: A Critical Review. *ACS Omega, 7*(11), 9088–9107. https://doi.org/10.1021/acsomega.2c00440
6. Nascimento, J. P. L., Teixeira, G. T. L., Obata, M. M. S., Silva, M. V., Oliveira, C. J. F., Silva, L. E. A., Gelamo, R. V., Slade, N. B. L., & Moreto, J. A. (2023). Influence of Reactive Sputtering-Deposited Nb<Subscript>2</Subscript>O<Subscript>5</Subscript> Coating On the Ti-6Al-4V Alloy Surfaces: Biomineralization, Antibacterial Activity, and Cell Viability Tests. *Materials Research, 26*, Article e2023025. https://doi.org/10.1590/1980-5373-MR-2023-0251
7. Moreto, J. A., Gelamo, R. V., da Silva, M. V., Steffen, T. T., de Oliveira, C. J. F., de Almeida Buranello, P. A., & Pinto, M. R. (2021). New insights of Nb<Subscript>2</Subscript>O<Subscript>5</Subscript>-based coatings on the 316L SS surfaces: Enhanced biological responses. *Journal Of Materials Science: Materials In Medicine, 32*(3), Article 25. https://doi.org/10.1007/s10856-021-06498-7
8. de Almeida Bino, M. C., Eurídice, W. A., Gelamo, R. V., Leite, N. B., da Silva, M. V., de Siervo, A., de Almeida Buranello, P. A., & Moreto, J. A. (2021). Structural and morphological characterization of Ti6Al4V alloy surface functionalization based on Nb<Subscript>2</Subscript>O<Subscript>5</Subscript> thin film for biomedical applications. *Applied Surface Science, 557*, Article 149739. https://doi.org/10.1016/j.apsusc.2021.149739
9. Marins, N. H., Silva, R. M., Ferrua, C. P., Łukowiec, D., Barbosa, A. M., Ribeiro, J. S., Nedel, F., Zavareze, E. R., Tański, T., & Carreño, N. L. (2020). Fabrication of electrospun poly(lactic acid) nanoporous membrane loaded with Niobium pentoxide nanoparticles as a potential scaffold for biomaterial applications. *J Biomed Mater Res B Appl Biomater*, *108*(4), 1559–1567. https://doi.org/10.1002/jbm.b.34503
10. Marins, N. H., Meereis, C. T., Silva, R. M., Ruas, C. P., Takimi, A. S., Carreño, N. L., & Ogliari, F. A. (2018). Radiopaque dental adhesive with addition of niobium pentoxide nanoparticles. *Polymer Bulletin, 75*, 2301–2314. https://doi.org/10.1007/s00289-017-2150-8
11. Pereira, T. A. V. Nanopartículas de óxidos de ferro e nióbio com diferentes recobrimentos: síntese, caracterização e avaliação do potencial biológico. Ph.D., & Thesis (2018). University of São Paulo. https://doi.org/10.11606/T.46.2019.tde-16042019-084916
12. Oliveira, P. A., Farnesi-de-Assunção, T. S., Rotta, I. S., Vicentine, K. F. D., Paiva, A. D., dos Santos Alvares, D., Teodoro, M. D., Wolf, W., Moreto, J. A., & Slade, N. B. L. (2025). Functionalization of nanostructured Niobium oxide with natural antioxidants for biomedical purposes. *Emergent Mater*, 1–17. https://doi.org/10.1007/s42247-025-01172-y
13. de Moraes, N. P., Silva, F. N., da Silva, M. L. C. P., Campos, T. M. B., Thim, G. P., & Rodrigues, L. A. (2018). Methylene blue photodegradation employing hexagonal prism-shaped niobium oxide as heterogeneous catalyst: Effect of catalyst dosage, dye concentration, and radiation source. *Materials Chemistry and Physics, 214*, 95–106. https://doi.org/10.1016/j.matchemphys.2018.04.063
14. de Melo Gues, A. P., De Miranda, D. L. R. T., Gondim, A. D., & Junior, C. G. L. (2024). Niobium pentoxide as an acid catalyst: An overview. *Journal of Engineering and Exact Sciences, 10*(7), Article 19766. https://doi.org/10.18540/jcecvl10iss7pp19766
15. Fan, W., Zhang, Q., Deng, W., & Wang, Y. (2013). Niobic acid nanosheets synthesized by a simple hydrothermal method as efficient Brønsted acid catalysts. *Chemistry of Materials*, *25*(16), 3277–3287. https://doi.org/10.1021/cm400192q
16. Hara, M. (2014). Heterogeneous Lewis acid catalysts workable in water. *Bulletin. Chemical Society of Japan*, *87*(9), 931–941. https://doi.org/10.1246/bcsj.20140131
17. Marin, M. L., Hallett-Tapley, G. L., Impellizzeri, S., Fasciani, C., Simoncelli, S., Netto-Ferreira, J. C., & Scaiano, J. C. (2014). Synthesis, acid properties and catalysis by niobium oxide nanostructured materials. *Catalysis Science & Technology, 4*(9), 3044–3052. https://doi.org/10.1039/C4CY00238E
18. Skrodczky, K., Antunes, M. M., Han, X., Santangelo, S., Scholz, G., Valente, A. A., Pinna, N., & Russo, P. A. (2019). Niobium pentoxide nanomaterials with distorted structures as efficient acid catalysts. *Communications Chemistry, 2*, Article 129. https://doi.org/10.1038/s42004-019-0231-3
19. Rodrigues, L. A., & da Silva, M. L. C. P. (2010). Synthesis of Nb<Subscript>2</Subscript>O<Subscript>5</Subscript>·nH<Subscript>2</Subscript>O nanoparticles by water-in-oil microemulsion. *Journal of Non-Crystalline Solids, 356*(3), 125–128. https://doi.org/10.1016/j.jnoncrysol.2009.11.002
20. Asencios, Y. J. O., & Machado, V. A. (2022). Photodegradation of organic pollutants in seawater and hydrogen production via methanol photoreforming with hydrated niobium pentoxide catalysts. *Sustainable Chemistry, 3*(2), 172–191. https://doi.org/10.3390/suschem3020012
21. Shah, S. T., Yehye, W. A., Saad, O., Simarani, K., Chowdhury, Z. Z., Alhadi, A. A., & Al-Ani, L. A. (2017). Surface functionalization of iron oxide nanoparticles with gallic acid as potential antioxidant and antimicrobial agents. *Nanomaterials, 7*(10), Article 306. https://doi.org/10.3390/nano7100306
22. Shah, S. T., Yehye, W. A., Saad, O., Simarani, K., Chowdhury, Z. Z., Alhadi, A. A., & Al-Ani, L. A. (2019). Magnetically directed antioxidant and antimicrobial agent: Synthesis and surface functionalization of magnetite with quercetin. *PeerJ, 7*, Article e7651. https://doi.org/10.7717/peerj.7651
23. Odzak, N., Kistler, D., Behra, R., & Sigg, L. (2014). Dissolution of metal and metal oxide nanoparticles in aqueous media. *Environmental Pollution*, *191*, 132–138. https://doi.org/10.1016/j.envpol.2014.04.010
24. Studer, A. M., Limbach, L. K., Van Duc, L., Krumeich, F., Athanassiou, E. K., Gerber, L. C., Moch, H., & Stark, W. J. (2010). Nanoparticle cytotoxicity depends on intracellular solubility: Comparison of stabilized copper metal and degradable copper oxide nanoparticles. *Toxicology Letters, 197*(3), 169–174. https://doi.org/10.1016/j.toxlet.2010.05.012
25. Teixeira, G. T. L., Gelamo, R. V., Obata, M. M. S., de Andra Silva, L. E., da Silva, M. V., de Oliveira, C. J. F., da Silva, B. P., Aoki, I. V., Moreto, J. A., & Slade, N. B. L. (2023). Exploring the functionalization of Ti-6Al-4V alloy with the novel antimicrobial peptide JIChis-2 via plasma polymerization. *Biofouling, 39*(1), 47–63. https://doi.org/10.1080/08927014.2023.2183121
26. Custódio, L., Mendes, L. A., dos Santos Alvares, D., Moreto, J. A., & Slade, N. B. L. (2022). Charge and rigidity effects on the encapsulation of quercetin by multilamellar vesicles. *Bulletin of Materials Science, 45*, Article 159. https://doi.org/10.1007/s12034-022-02734-0
27. Leite, N. B., dos Santos Alvares, D., de Souza, B. M., Palma, M. S., & Ruggiero Neto, J. (2014). Effect of the aspartic acid D2 on the affinity of Polybia-MP1 to anionic lipid vesicles. *European*

Biophysics Journal : EBJ, 43, 121–130. https://doi.org/10.1007/s00249-014-0945-1
28. International Organization for Standardization (ISO). (2009). *ISO 10993-5:2009. Biological evaluation of medical devices-part 5: Tests for in vitro cytotoxicity*. ISO.
29. Borenfreund, E., & Puerner, J. A. (1985). Toxicity determined *in vitro* by morphological alterations and neutral red absorption. *Toxicology Letters, 24*(2–3), 119–124. https://doi.org/10.1016/0378-4274(85)90046-3
30. Rogero, S. O., Lugão, A. B., Ikeda, T. I., & Cruz, Á. S. (2003). Teste *in vitro* de citotoxicidade: Estudo comparativo entre duas metodologias. *Materials Research, 6*, 317–320. https://doi.org/10.1590/S1516-14392003000300003
31. Madorran, E., Ambrož, M., Knez, J., & Sobočan, M. (2025). An overview of the current state of cell viability assessment methods using OECD classification. *International Journal of Molecular Sciences, 26*(1), Article 220. https://doi.org/10.3390/ijms26010220
32. Madorran, E., Stožer, A., Bevc, S., & Maver, U. (2020). *In vitro* toxicity model: Upgrades to bridge the gap between preclinical and clinical research. *Biomolecules & Biomedicine, 20*(2), 157–168. https://doi.org/10.17305/bjbms.2019.4378
33. Clinical and Laboratory Standards Institute (CLSI). (2023). *CLSI supplement M100, performance standards for antimicrobial susceptibility testing* (33rd ed.). CLSI.
34. Clinical and Laboratory Standards Institute (CLSI). (2020). *CLSI supplement M100, performance standards for antimicrobial susceptibility testing* (30th ed.). CLSI.
35. Rocha, K. R., Perini, H. F., de Souza, C. M., Schueler, J., Tosoni, N. F., Furlaneto, M. C., & Furlaneto-Maia, L. (2019). Inhibitory effect of bacteriocins from enterococci on developing and preformed biofilms of *Listeria monocytogenes*, *Listeria ivanovii* and *Listeria innocua*. *World Journal of Microbiology & Biotechnology, 35*, Article 96. https://doi.org/10.1007/s11274-019-2675-0
36. Rodrigues, L. A. (2009). Síntese de nanopartículas de óxido de nióbio hidratado via microemulsão inversa. M.S. Dissertation, University of São Paulo. https://doi.org/10.11606/D.97.2009.tde-03102012-121612
37. Chen, X., Yu, T., Fan, X., Zhang, H., Li, Z., Ye, J., & Zou, Z. (2007). Enhanced activity of mesoporous Nb<Subscript>2</Subscript>O<Subscript>5</Subscript> for photocatalytic hydrogen production. *Applied Surface Science, 253*(20), 8500–8506. https://doi.org/10.1016/j.apsusc.2007.04.035
38. Ristić, M., Popović, S., & Musić, S. (2004). Sol–gel synthesis and characterization of Nb<Subscript>2</Subscript>O<Subscript>5</Subscript> powders. *Materials Letters, 58*(21), 2658–2663. https://doi.org/10.1016/j.matlet.2004.03.041
39. Souza, C. R., da Silva, L. M., Penha, F. M., & Rocha, S. D. F. (2025). Crystallization-based recovery of niobium compounds from alkaline liquor. *Separation and Purification Technology, 360*, Article 131085. https://doi.org/10.1016/j.seppur.2024.131085
40. Fuchigami, T., & Kakimoto, K. I. (2017). Spiky niobium oxide nanoparticles through hydrothermal synthesis. *Journal of Materials Research, 32*, 3326–3332. https://doi.org/10.1557/jmr.2017.200
41. Huang, X., & El-Sayed, M. A. (2010). Gold nanoparticles: Optical properties and implementations in cancer diagnosis and photothermal therapy. *Journal of Advanced Research*, *1*(1), 13–28. https://doi.org/10.1016/j.jare.2010.02.002
42. Salim, E. T., Shafeeq, S. R., AbdulRazzaq, M. J., Fakhri, M. A., & Gopinath, S. C. (2023). Photo-activation of Ag chemicals for enhanced Nb<Subscript>2</Subscript>O<Subscript>5</Subscript> optoelectronic device employing plasmonic effects. *Surfaces and Interfaces, 36*, Article 102618. https://doi.org/10.1016/j.surfin.2022.102618
43. Ambreen, S., Pandey, N. D., Chouhan, A., Kumar, H., & Pandey, A. (2021). Effect of chelation in alkoxide precursors of niobium oxide nanoparticles on photochemical degradation of rhodamine B. *Journal of Sol-Gel Science and Technology, 98*, 319–334. https://doi.org/10.1007/s10971-021-05514-0
44. Uekawa, N., Kudo, T., Mori, F., Wu, Y. J., & Kakegawa, K. (2003). Low-temperature synthesis of niobium oxide nanoparticles from peroxo niobic acid sol. *Journal of Colloid and Interface Science, 264*(2), 378–384. https://doi.org/10.1016/S0021-9797(03)00460-0
45. Stuart, B. H. (2004). *Infrared Spectroscopy: Fundamentals and Applications* (1st ed). John Wiley & Sons.
46. Burke, P. A., & Ko, E. I. (1991). Acidic properties of oxides containing niobia on silica and niobia in silica. *Journal of Catalysis, 129*(1), 38–46. https://doi.org/10.1016/0021-9517(91)90007-Q
47. Engel, R. G., Kriz, G. S., Lampman, G. M., & Pavia, D. L. (2011). *Introduction to Organic Laboratory Techniques: Small Scale Approach* (3rd ed). Cengage Learning.
48. Bousada, G. M., da Silva, V. N., de Souza, B. F., de Oliveira, R. S., Junior, I. M., da Cunha, C. H. F., Astruc, D., Teixeira, R. R., & Moreira, R. P. L. (2024). Niobic acid as a support for microheterogeneous nanocatalysis of sodium borohydride hydrolysis under mild conditions. *RSC Advances, 14*, 19459–19471. https://doi.org/10.1039/D4RA01879F
49. Pavia, D. L., Lampman, G. M., Kriz, G. S., & Vyvyan, J. R. (2008). *Introduction to Spectroscopy* (4th ed). Cengage Learning.
50. Shen, F., Sun, Z., He, Q., Sun, J., Kaner, R. B., & Shao, Y. (2021). Niobium pentoxide based materials for high rate rechargeable electrochemical energy storage. *Materials Horizons*, *8*, 1130–1152. https://doi.org/10.1039/D0MH01481H
51. Zhang, X., Wang, H., & Luo, L. (2022). Comparison analysis of the calculation methods for particle diameter. *Crystals, 12*(8), Article 1107. https://doi.org/10.3390/cryst12081107
52. Shanthi, C., Porpatham, R. K., & Pappa, N. (2014). Image analysis for particle size distribution. *International Journal of Engineering & Technology, 6*(3), 1340–1345.
53. Zhang, S., & Wang, C. (2023). Precise analysis of nanoparticle size distribution in TEM image. *Methods and Protocols, 6*(4), Article 63. https://doi.org/10.3390/mps6040063
54. Kumari, N., Samdarshi, S. K., Verma, R., Gaurav, K., Bhattacharyya, A. S., Mohanty, K., & Deshpande, U. (2023). Superior functionality of niobium pentoxide nano-rod/tripod photocatalyst synthesized using polyethyleneimine as a soft template for the abatement of methylene blue under UV and visible irradiation. *Environmental Science and Pollution Research, 30*, 122458–122469. https://doi.org/10.1007/s11356-023-31001-w
55. Kumari, N., Gaurav, K., Samdarshi, S. K., Bhattacharyya, A. S., Paul, S., Rajbongshi, B., & Mohanty, K. (2020). Dependence of photoactivity of niobium pentoxide (Nb<Subscript>2</Subscript>O<Subscript>5</Subscript>) on crystalline phase and electrokinetic potential of the hydrocolloid. *Solar Energy Materials and Solar Cells, 208*, Article 110408. https://doi.org/10.1016/j.solmat.2020.110408
56. Mendes, L. A., Farnesi-de-Assunção, T. S., Oliveira, P. A., Rotta, I. S., Moreto, J. A., Devienne, K. F., Paiva, A. D., & Slade, N. B. L. (2024). Antitumor potential of lipid nanoformulations with natural antioxidants. *Nano Trends, 7*, Article 100040. https://doi.org/10.1016/j.nwnano.2024.100040
57. Erhirhie, E. O., Ihekwereme, C. P., & Ilodigwe, E. E. (2018). Advances in acute toxicity testing: Strengths, weaknesses and regulatory acceptance. *Interdisciplinary Toxicology, 11*(1), 5–12. https://doi.org/10.2478/intox-2018-0001
58. Ates, G., Vanhaecke, T., Rogiers, V., & Rodrigues, R. M. (2017). Assaying Cellular Viability Using the Neutral Red Uptake Assay. In D. Gilbert & O. Friedrich (Eds.), *Cell Viability Assays:*

Methods in Molecular Biology (pp. 19–26). https://doi.org/10.1007/978-1-4939-6960-9_2
59. Kurutas, E. B. (2015). The importance of antioxidants which play the role in cellular response against oxidative/nitrosative stress: Current state. *Nutrition Journal, 15*, Article 71. https://doi.org/10.1186/s12937-016-0186-5
60. Pinheiro, L. D. S. M., Sangoi, G. G., Vizzotto, B. S., Ruiz, Y. P. M., Galembeck, A., Pavoski, G., Espinosa, D. C. R., Machado, A. K., & da Silva, W. L. (2024). Silver nanoparticles from ascorbic acid: Biosynthesis, characterization, *in vitro* safety profile, antimicrobial activity and phytotoxicity. *Materials Chemistry and Physics, 325*, Article 129715. https://doi.org/10.1016/j.matchemphys.2024.129715
61. Yarjanli, Z., Ghaedi, K., Esmaeili, A., Zarrabi, A., & Rahgozar, S. (2019). The antitoxic effects of Quercetin and Quercetin-conjugated iron oxide nanoparticles (QNPs) against H_2O_2-induced toxicity in PC12 cells. *International Journal of Nanomedicine, 14*, 6813–6830. https://doi.org/10.2147/IJN.S212582
62. Daré, R. G., Kolanthai, E., Neal, C. J., Fu, Y., Seal, S., Nakamura, C. V., & Lautenschlager, S. O. (2023). Cerium oxide nanoparticles conjugated with tannic acid prevent UVB-induced oxidative stress in fibroblasts: Evidence of a promising anti-photodamage agent. *Antioxidants, 12*(1), Article 190. https://doi.org/10.3390/antiox12010190
63. Dsouki, N. A., de Lima, M. P., Corazzini, R., Gáscon, T. M., Azzalis, L. A., Junqueira, V. B. C., Feder, D., & Fonseca, F. L. A. (2014). Cytotoxic, hematologic and histologic effects of niobium pentoxide in Swiss mice. *Journal of Materials Science: Materials in Medicine, 25*, 1301–1305. https://doi.org/10.1007/s10856-014-5153-0
64. Kiyochi Junior, H. D. J., Candido, A. G., Bonadio, T. G. M., Da Cruz, J. A., Baesso, M. L., Weinand, W. R., & Hernandes, L. (2020). In vivo evaluation of interactions between biphasic calcium phosphate (BCP)-niobium pentoxide (Nb_2O_5) nanocomposite and tissues using a rat critical-size calvarial defect model. *Journal of Materials Science: Materials in Medicine, 31*, Article 71. https://doi.org/10.1007/s10856-020-06414-5
65. Costerton, J. W., Stewart, P. S., & Greenberg, E. P. (1999). Bacterial biofilms: A common cause of persistent infections. *Science, 284*(5418), 1318–1322. https://doi.org/10.1126/science.284.5418.1318
66. Nair, M. S., Upadhyay, A., Fancher, S., Upadhyaya, I., Dey, S., Kallanoor-Johny, A., Zhao, J., & Venkitanarayanan, K. (2018). Inhibition and inactivation of *Escherichia coli* O157: H7 biofilms by selenium. *Journal of Food Protection, 87*, 926–933. https://doi.org/10.4315/0362-028X.JFP-17-427
67. Xu, J., Li, Y., Wang, H., Zhu, M., Feng, W., & Liang, G. (2021). Enhanced antibacterial and anti-biofilm activities of antimicrobial peptides modified silver nanoparticles. *International Journal of Nanomedicine, 16*, 4831–4846. https://doi.org/10.2147/IJN.S315839
68. Guo, S., Liu, X., Chen, H., Wang, J., Qiao, Y., Zhang, T., Ji, X., Han, H., Liu, Z., Bai, Y., & Tang, J. (2024). Antibacterial effect of the metal nanocomposite on *Escherichia coli*. *Journal of Hazardous Materials, 476*, Article 135149. https://doi.org/10.1016/j.jhazmat.2024.135149
69. Mahmudin, L., Wulandani, R., Riswan, M., Kurnia, S. E., Dwi, J. P., Syahrul, U. M., Arifin, M., & Suharyadi, E. (2024). Silver nanoparticles-based localized surface plasmon resonance biosensor for *Escherichia coli* detection. *Spectrochimica Acta. Part A, Molecular and Biomolecular Spectroscopy, 311*, Article 123985. https://doi.org/10.1016/j.saa.2024.123985
70. Szymczak, M., & Golec, P. (2024). Long-term effectiveness of engineered T7 phages armed with silver nanoparticles against *Escherichia coli* biofilm. *International Journal of Nanomedicine, 19*, 10097–10105. https://doi.org/10.2147/IJN.S479960
71. Yang, N., Wu, T., Li, M., Hu, X., Ma, R., Jiang, W., Su, Z., Yang, R., & Zhu, C. (2024). Silver-quercetin-loaded honeycomb-like Ti-based interface combats infection-triggered excessive inflammation via specific bactericidal and macrophage reprogramming. *Bioactive Materials, 43*, 48–66. https://doi.org/10.1016/j.bioactmat.2024.09.012
72. Al-Sawarees, D. K., Darwish, R. M., Abu-Zurayk, R., & Masri, M. A. (2024). Assessing silver nanoparticle and antimicrobial combinations for antibacterial activity and biofilm prevention on surgical sutures. *Journal of Applied Microbiology, 135*(4), Article lxae063. https://doi.org/10.1093/jambio/lxae063
73. Norouzalinia, F., Asadpour, L., & Mokhtary, M. (2025). Antimicrobial, anti-biofilm, and efflux pump inhibitory effects of ellagic acid–bonded magnetic nanoparticles against *Escherichia coli* isolates. *International Microbiology, 28*, 563–573. https://doi.org/10.1007/s10123-024-00560-4

Authors and Affiliations

Pablo A. Oliveira[1] · Thaís S. Farnesi-de-Assunção[2] · Isabela S. Rotta[2] · Karina F. D. Vicentine[2] · Aline D. Paiva[2] · Dayane S. Alvares[3] · Witor Wolf[4] · Jéferson A. Moreto[4] · Natália B. L. Slade[1]

✉ Natália B. L. Slade
natalia.slade@uftm.edu.br

[1] Institute of Exact Sciences, Naturals and Education, Federal University of Triângulo Mineiro, Uberaba 38064-200, Minas Gerais, Brazil

[2] Institute of Biological and Natural Sciences, Federal University of Triângulo Mineiro, Uberaba 38025-350, Minas Gerais, Brazil

[3] Institute of Biosciences, Letters and Exact Sciences, São Paulo State University, São José do Rio Preto, São Paulo 15054-000, Brazil

[4] Department of Materials Engineering, São Carlos School of Engineering, University of São Paulo, São Carlos, São Paulo 13566-590, Brazil